Atmos. Meas. Tech. Discuss., 2, 1901–1931, 2009
www.atmos-meas-tech-discuss.net/2/1901/2009/

Atmospheric Measurement Techniques Discussions

Atmospheric Measurement Techniques Discussions is the access reviewed discussion forum of *Atmospheric Measurement Techniques*

Assessment of the performance of a compact concentric spectrometer system for Atmospheric Differential Optical Absorption Spectroscopy

C. Whyte[1], R. J. Leigh[1], D. Lobb[2], T. Williams[2], J. J. Remedios[1], M. Cutter[2], and P. S. Monks[3]

[1]Earth Observation Science, Space Research Centre, Department of Physics and Astronomy, University of Leicester, University Road, Leicester, LE1 7RH, UK
[2]Surrey Satellite Technology Ltd., Rayleigh House, 1 Bat and Ball Road, Sevenoaks, TN14 5LJ, UK
[3]Department of Chemistry, University of Leicester, University Road, Leicester, LE1 7RH, UK

Received: 23 July 2009 – Accepted: 28 July 2009 – Published: 6 August 2009

Correspondence to: P. S. Monks (psm7@le.ac.uk)

Published by Copernicus Publications on behalf of the European Geosciences Union.

Abstract

A breadboard demonstrator of a novel UV/VIS grating spectrometer for atmospheric research has been developed based upon a concentric arrangement of a spherical meniscus lens, concave spherical mirror and curved diffraction grating suitable for a range of remote sensing applications from the ground or space. The spectrometer is compact and provides high optical efficiency and performance benefits over traditional instruments. The concentric design is capable of handling high relative apertures, owing to spherical aberration and coma being near zero at all surfaces. The design also provides correction for transverse chromatic aberration and distortion, in addition to correcting for the distortion called "smile", the curvature of the slit image formed at each wavelength. These properties render this design capable of superior spectral and spatial performance with size and weight budgets significantly lower than standard configurations. This form of spectrometer design offers the potential for an exceptionally compact instrument for differential optical absorption spectroscopy (DOAS) applications particularly from space (LEO, GEO orbits) and from HAPs or ground-based platforms. The breadboard demonstrator has been shown to offer high throughput and a stable Gaussian line shape with a spectral range from 300 to 450 nm at better than 0.5 nm resolution, suitable for a number of typical DOAS applications.

1 Introduction

Measurement of atmospheric species with climate change or air quality (AQ) implications is a key driver for ground and space-based Earth Observation. Techniques such as differential optical absorption spectroscopy (DOAS) (Platt, 1994; Edner et al., 1993; Evangelisti et al., 1995; Veitel et al., 2002; Honninger et al., 2004; Lohberger et al., 2004; Lee et al., 2005; Friess et al., 2005; Sinreich et al., 2005) operating in the UV/Visible bandwidth have been used over a number of decades for the retrieval of atmospheric concentrations of such key parameters as ozone (O_3) (Axelsson et al.,

AMTD

2, 1901–1931, 2009

1990; Virkkula, 1997; Wang et al., 2006; Kim et al., 2007), nitrogen dioxide (NO_2) (Van Roozendael et al., 1994; Leser et al., 2003; Pundt et al., 2005; Palazzi et al., 2007; Louban et al., 2008; Kramer et al., 2008; Leigh et al., 2007), formaldehyde (HCHO) (Cardenas et al., 2000), the halogen oxides (bromine BrO – Richter et al., 1999; Aliwell et al., 2002; Honninger and Platt, 2002; Bobrowski et al., 2003; Bobrowski and Platt, 2007, chlorine OClO – Tornkvist et al., 2002; Kuhl et al., 2006 and iodine IO – Wittrock et al., 2000; Friess et al., 2001), and the oxygen dimer O_4 (Wagner et al., 2004; Friess et al., 2006; Leigh et al., 2007) from which information on the atmospheric aerosol profile can be retrieved.

NO_2, O_3, and HCHO are factors in air quality with impacts on human health, specifically being implicated in impaired lung function (Bonay and Aubier, 2007). In most scenarios the primary anthropogenic source of NO_2 is vehicular emission (Eskes et al., 2006). Typical concentrations of NO_2 range from 10–45 ppbV, elevated to 200 ppbV during high pollution episodes (DEFRA, 2007). Ozone is a secondary pollutant generated through the sunlight initiated oxidation of VOCs, including formaldehyde in the presence of nitrogen oxides (NO_x) (Monks, 2003). Typical concentrations are 15 ppbV, elevated to over 100 ppbV in hot and sunny conditions (DEFRA, 2007). Formaldehyde (and aldehydes in general) and glyoxal ($C_2H_2O_2$) (Hastings et al., 2005) have been implicated in the formation of components that produce photochemical smog.

There is a requirement for accurate measurement of such atmospheric species at high spatio-temporal resolution to accurately determine fluxes and map transport. Furthermore, to provide data for use in regional forecasting and monitoring it is necessary to interrogate the planetary boundary layer at a spatial resolution suitable for assimilation into mesoscale models, often 2 km by 2 km or less (Cai et al., 2002; Harrison et al., 2006; Mihailovic et al., 2005; Owen et al., 1999). The use of satellite data in such initiatives is constrained by difficulties in the retrieval of data from the PBL owing to the presence of clouds. A high spatial resolution significantly increases the likelihood of cloud free pixels that could be recorded, while simultaneously providing data on a quasi-urban scale (2–10 km). The abundance of many AQ species is driven

by photochemistry, showing significant diurnal variability, requiring systems with low noise and high throughput which offer relatively high temporal resolution. Compact instruments capable of providing the necessary optical performance and spectral resolution to make meaningful measurements of these target species are a key enabling technology.

In 1994 a design for a new type of optical concentric spectrometer based on an Offner relay spectrometer was published by Lobb (1994). A standard Offner spectrometer consists of three spherical concentric mirrors: two concave and one convex, sometimes with an added concentric meniscus lens. The object and image surfaces are typically in a common plane that includes the common centre of curvature (Prieto-Blanco et al., 2006). Lobb's configuration uses a single concave spherical mirror (from which light is reflected twice) and a spherical meniscus lens. The convex mirror is replaced by a convex spherical diffraction grating. The spectrally-dispersed image is again in the same plane as the common centre. The grating pattern lines are in equi-spaced parallel planes orthogonal to the focal plane (Lobb, 2004). A schematic diagram of such a system is given in Fig. 1. This concept could allow for a high performance imaging spectrometer of a considerably reduced size compared to equivalent instrumentation (in a Czerny-Turner configuration for example).

The beam from the entrance slit is folded at a flat mirror and passes through the meniscus lens, where it is then reflected by the concave mirror, and falls on the grating. A first order diffracted beam forms the useful spectral image from the second reflection at the concave spherical mirror and second transmission through the meniscus lens. The design requires a grating frequency in the order of >2000 cycles/mm for UV/Visible applications and features relatively large diffractive deflections, which makes the system compact with an intrinsic stability of wavelength calibration. This optical arrangement inherently leads to near zero spherical aberration (Lobb, 2004). Full details can be found in (Lobb, 1994, 2004) and (Bovensmann et al., 2002, 2004).

The concentric spectrometer concept could provide a compact and powerful instrument for differential optical absorption spectroscopy (DOAS) applications for ground

AMTD
2, 1901–1931, 2009

based observations, high altitude platforms (HAP) or for satellite imaging. This paper details the characterisation of the first DOAS demonstrator of this novel concentric spectrometer system, including details on the optical components and an appraisal of the performance of the instrument in comparison to target specifications.

2 Experimental design

A concentric spectrometer was first proposed for space flight as part of a ESA study (Bovensmann et al., 2004), however the technology had not been practically demonstrated. The specifications for this design were predicated on potential flight opportunities for such an instrument and as such the demonstrator was designed as a representation of a low earth orbit space based system with daily global coverage (swath width 2600 km).

To demonstrate the operational capabilities of this design the demonstrator was conceived as a broadband imaging spectrometer with the primary objective of the detection of the key air quality significant atmospheric species: NO_2 and tropospheric O_3 over an operational bandwidth of 300–450 nm. This bandwidth also permits the detection of other important trace gases, such as HCHO, glyoxal and BrO and provides a measure of the aerosol optical thickness through retrievals of the oxygen dimer, O_4. The emphasis on the detection of atmospheric compounds with significance to air quality monitoring resulted in this novel spectrometer being attributed with the acronym Compact Air Quality Spectrometer, or CompAQS.

A driver for the design was that of representing a LEO (Low Earth Orbit) imaging system with global daily coverage suitable for air quality applications. To produce a 5×5 km ground pixel over a 2500 km swath width, a spatial resolution of 90 μm over the 52 mm length of the entrance slit was specified, giving over 500 resolved elements. The target along-track resolution and orbit constrains the sampling time to be less than 0.8 s. A spectral resolution of 0.5 nm is sufficient for DOAS retrievals of the target species, while a sampling factor of 7 pixels per FWHM provides sufficient detail to assess the

AMTD
2, 1901–1931, 2009

instrument line shape in both spectral and spatial domains. Taking these factors into account the CompAQS demonstrator was designed with a focal plane consisting of 2048 spectral pixels, giving spectral sampling of 0.075 nm per pixel, and 4096 spatial pixels with a corresponding spatial sampling of 13 μm (650 m from LEO) per pixel. The relative aperture at the slit is $f/3.06$ in the spectral domain, $f/1.25$ in the spatial domain, and the spectrometer has unit magnification, such that the width of the entrance slit is the same as the FWHM of a resolved spectral element on the focal plane. The target operational specifications described above determine the size and layout of the CompAQS demonstrator. The conceptual driver for the spectrometer is such that the size of the optical components, including the radius of curvature of the grating, lens and mirror, scale linearly with the size of the focal plane.

The detector package used in the demonstrator was an e2V CCD48–20 Back Illuminated CCD sensor with a 1.3×1.3 cm active area detector, comprising an array of 1024×1024, 13×13 μm pixels, with an associated electron capacity of up to 100 000 electrons per pixel. This pixel size determined the focal plane to be 27.6×55.2 mm in size. The CCD was translated through a 2× array to map the full focal plane. Owing to the spatial relationship between the optical components and the size of the focal plane the resultant dimensions for the arrangement of the optical components and the focal plane result in a volume which is little over 20 cm cubed.

2.1 Diffraction grating

Of the bespoke optical elements the diffraction grating had the most exacting manufacturing tolerances owing to its impact on instrument throughput, with the lowest transmission of all the optical components and the strongest potential for stray light if not manufactured accurately. To provide the necessary spectral sampling over the bandwidth of the CompAQS demonstrator the grating required a grating frequency of 2350±1 cycles/mm. The grating was manufactured by Carl Zeiss Optronics GmbH from a fused silica substrate provided by Comar Instruments (UK), polished to an RMS smoothness of 0.40 nm across the optical surface. The diffraction efficiency was

AMTD
2, 1901–1931, 2009

relatively uniform for non-polarised light across the bandwidth, with a mean efficiency of 60% from the half-sinusoidal profile. Analysis performed by Carl Zeiss showed that the error in the groove direction was ±0.06 degrees. The micro-roughness of the grating surface was evaluated by Carl Zeiss using AFM measurements made across the surface. The mean micro roughness, σ, was 0.93 nm with an intrinsic error of ±0.1 nm rms. To provide a cursory evaluation into the quality of the grating the total integrated scatter ($[4\pi\sigma/\lambda]^2$) from the grating surface was calculated across the bandwidth and was shown to vary smoothly from approximately 0.15% at the lower end of the target bandwidth to approximately 0.07% at the upper end of the bandwidth. The grating marks a significant achievement in that a high-quality, technically demanding grating can be manufactured on a convex surface with a relatively small radius of curvature for implementation in this novel technology.

2.2 Spherical meniscus lens, concave spherical mirror and fold mirror

The spherical lens and mirror were manufactured by the Florida based company Coastal Optical Systems (US), fabricated from fused silica. The lens was anti-reflection coated; measurements on each side of the lens showed that the reflectivity was below 0.5% over the majority of the bandwidth, with a local minimum of approximately 0.01% between 350 and 400 nm and a maximum of approximately 0.9% at 450 nm, at which point the reflectivity rose sharply outside of the demonstrator bandwidth. The mirror was coated with a dielectric-protected aluminium layer provided by Universal Thin Film Labs. The reflective coating gave a total reflectivity of between 91 and 93% over the bandwidth, with the local maximum at approximately 350 nm. The optical surfaces of each item were analysed by Coastal Optical Systems using optical interferometry. The front surface of the lens was measured to have a RMS micro-roughness of 0.417 nm while the rear surface had a value of 0.276 nm. While there has been no appraisal of the subsurface quality of the lens the total integrated scatter has been reasonably assumed to be less than 0.1% across the bandwidth accounting for light passing twice through the lens in the instrument (from source to grating, from grating to detector). The

AMTD
2, 1901–1931, 2009

RMS micro-roughness of the finished optical surface of the concave mirror was found to be 0.491 nm, giving a total integrated scatter under 0.09% over the bandwidth, again accounting for light reflecting twice off the mirror surface.

The fold mirror was provided by SP3 Plus (UK), again made from fused silica with a reflective aluminium and protective dielectric coating, with a specified surface polish of 1 nm. The total reflectivity was measured to be between approximately 92 and 92.5% across the bandwidth, with the local maximum appearing at approximately 440 nm. The combined total integrated scatter for the current instrument is given in Table 1.

The estimated total integrated scatter of the instrument is shown to decrease with increasing wavelength, and these values can provide a rough estimate of the total fraction of stray light that may be generated from the optical components, with 0.51% to 0.28% of the total incident photons deviating from the intended light path, of which a portion may terminate at the focal plane. Stray light is a significant issue for scattered sunlight systems. As a demonstrator for a LEO system CompAQS was designed to work with typical Earth spectral radiance levels, which increases over the operational bandwidth by some three orders of magnitude (Kelder et al., 2005) from 1.7×10^{11} to 1.5×10^{14} photons/[cm^2.s. sr. nm]. Therefore stray light from longer wavelength radiation can obscure the weaker, lower wavelength radiation, leading to poor quality data from the UV channels. This current iteration of the concentric spectrometer was intended primarily as a demonstrator of the concentric spectrometer concept and as such the overall quality of the components is not necessarily representative of the requirements of a true space instrument nor the ultimate performance achievable for such items.

AMTD
2, 1901–1931, 2009

3 Results

The following section describes the experiments to investigate and characterise the demonstrator system, and the outcomes of this analysis in comparison to the target performance.

The demonstrator did not include an entrance telescope system. Light enters the instrument through a square-conical baffle with the entrance slit at the apex of the cone. Two entrance slits were used with widths of 65 and 78 μm. Owing to the tight spatial constraints in front of the focal plane, it was not possible to provide a cover window over the CCD surface, and the CCD system could not be evacuated and was cooled to ~12°C by a Peltier cooler.

The concentric components were initially aligned by adjusting the position of each component to optimise the detection of mercury emission lines, and the alignment refined through the use of an adapted autocollimator. For the initial alignment experiments light from an Ocean Optics HG-1 Mercury Argon Calibration Source was passed through a 1 mm diameter optical fibre positioned approximately 30 mm from the centre of the entrance slit, such that the light filled the entrance slit. This light provided a means of checking the alignment of the instrument in terms of bandwidth covered by the focal plane, the focus of the instrument, the instrument line shape and wavelength calibration. The 65 and 78 μm slits were fitted and experiments carried out with both using an integration time of one second.

Through an iterative tuning process the spectrometer was optimised to record spectra showing the 365.02, 366.33, 404.66, and 407.78 nm lines of the mercury spectrum, and on moving the CCD in the spectral domain the 435.84 nm line.

It was possible to assess the instrument line shape by examining cut sections of the CCD image, such as those shown in Fig. 2 for the emission lines recorded using the 78 μm slit. Each emission line was examined in detail with Fig. 3 showing the 365 nm peak recorded using a slit width of 65 and 78 μm respectively. The 65 μm (0.065 nm) slit offers a finer resolution, with a FWHM of between 4 and 5 pixels. Using the 78 μm

AMTD
2, 1901–1931, 2009

(0.078 nm) slit the 365.02 and 365.48 nm lines could not be resolved, although the FWHM matched the expected 6–7 pixels for this slit width. Fig. 3 also shows Gaussian fits made to each peak, generated with MicroCal Origin V6 software. The R^2 values for each fit are mostly in excess of 0.99, confirming the stability of the Gaussian line shape across the spectral domain, a key requirement for DOAS. Figure 4 shows similar plots with the 404 and 407 nm lines.

The wavelengths of the emission lines were attributed to the location of the peak centres on the CCD, and from this data a wavelength calibration for the instrument for both slit widths was determined, as given in Fig. 5. The calibration data demonstrates a strong linear relationship between the line position on the CCD and wavelength, with the data from the 65 μm slit having a slightly better correlated linear fit than that from the 78 μm slit. From this data it was possible to determine the spectral sampling characteristics for both slits: the effective sampling of the instrument with the 65 μm (0.065 nm) slit was 0.07044 nm/pixel, and 0.07000 nm/pixel with the 78 μm (0.078) slit. The spectrometer bandwidth covered 150 nm in around 2150 pixels in a spatial distance of approximately 27.7 mm, marginally larger than the design specification of 27.6 mm. Applying the wavelength calibrations to the recorded data allowed evaluation of the spectral resolution of the recorded emission lines. Figure 6 shows the corresponding wavelength calibrated data recorded with the 65 μm slit, with new Gaussian fits giving a spectral resolution of approximately 0.3 nm. The corresponding spectral resolution for the 78 μm slit was approximately 0.45 nm.

The spectral sampling was re-assessed using an autocollimator through a two step process. The autocollimator (Taylor Hobson, Microptic TA50 142/12) was fitted with an objective lens to focus the light emitted from the autocollimator. The autocollimator was adjusted to give a single point reflection from the grating surface, such that the point of focus was on the shared centre of curvature. The spherical meniscus lens was then introduced into the system and adjusted to give a coincident reflection from the meniscus lens front surface, as illustrated in Fig. 7a). The autocollimator was then moved and a single point reflection sought from the rear surface of the meniscus lens.

AMTD
2, 1901–1931, 2009

The concave mirror was introduced and adjusted so as to give a coincident reflection, as shown in Fig. 7b).

Once aligned the other components were fitted and aligned. Using the 65 μm entrance slit spectra were recorded using a mercury lamp (Oriel 65160 with power supply 65150) positioned 30 cm from the entrance slit, passing through a diffuser prior to entering the spectrometer. Spectra were recorded in the same manner as before. A wavelength calibrated spectrum of emission lines from 365.02–435.84 nm is shown in Fig. 8.

Figure 9 shows the 365 nm emission lines with an identical FWHM of 4 pixels/0.3 nm as determined previously and the Gaussian fits applied to the emission lines have a range of R^2 values between 0.95 and 0.99. The spatial sampling of the demonstrator was appraised by passing another slit of known width perpendicular to the entrance slit to create an entrance aperture of known dimensions. The resultant light on the focal plane covers a set number of pixels in the spatial domain equivalent to the width of the perpendicular slit. The same instrument configuration was used as before to allow for a direct comparison with the previous work to assess the spectral characteristics of the instrument. The 68 μm slit was used as the entrance slit and a 91 μm slit was used as the perpendicular slit for this experiment.

The perpendicular slit was placed at fixed points along the entrance slit relative to its centre (−20 mm, −10 mm, 0, +10 mm, +20 mm from the centre) and measurements made. The 404.66 nm emission line was the target for these experiments. With the perpendicular slit in place the emission line was found to retain the Gaussian spectral line shape with a consistent fitting R^2 value of 0.996. Figure 10 shows the spatially resolved peaks from the same emission line at different points along the entrance slit. The FWHM for these peaks is 6 to 7 pixels.

The individually resolved points were imaged in 3-D to appraise their shape, both spectrally and spatially, and the surrounding background levels of noise. Figure 11 shows such a plot for the 404.66 nm central spot. With a spatial aperture of 91 μm and a single pixel size of 13 μm the FWHM of the spatially resolved element was confirmed

AMTD
2, 1901–1931, 2009

as 7 pixels providing over 500 resolved elements over the 52 mm entrance slit. With the current focal plane size and appropriate entrance optics, a LEO system with a global coverage swath width of 2600 km would have a resultant spatial sampling of 650 m, with an across-swath ground resolution of approximately 5 km.

One key advantage of the concentric spectrometer design is the lack of curvature in the image of the entrance slit on the focal plane, an effect known as smile. A preliminary measurement of the smile of the CompAQS breadboard demonstrator was made by illuminating the full entrance slit with the Hg-Ar lamp. The resulting spectral line, imaged across the spatial domain was analysed for linearity across the detector. The results are shown in Fig. 12. Although some minor deviations from a linear response are suggested, the deviations are less than half of a 13 μm pixel across the entire 13 mm CCD surface.

Although entrance optics were not incorporated into the CompAQS demonstrator, a rudimentary system was tested using a fibre optic input and convex lenses to image scattered sunlight into the CompAQS instrument. The resulting spectrum is given in Fig. 13, plotted with a Kurucz solar spectrum. Using the established WinDOAS analysis package, the FWHM of this spectrum was measured at 0.55 nm, with a linear wavelength calibration confirming the sampling of 0.0705±0.001 nm/pixel. This demonstrates that even at this preliminary stage of development CompAQS should be a powerful tool for future DOAS work.

4 Conclusions

The concentric spectrometer (CompAQS) concept theoretically offers exceptional spatial and spectral performance at very low volume and weight budgets, and the demonstrator has confirmed those key features: the volume of the optical components and focal plane in the demonstrator is little bigger than 20 cm cubed, and the instrument provides sufficiently high spectral and spatial sampling intervals to allow for oversampling factors of 7 pixels with a relatively high spectral resolution of 0.5 nm and 5 km

AMTD
2, 1901–1931, 2009

across-track spatial resolution. The instrument line shape has been characterised and shown to approximate a Gaussian profile with measured R^2 values typically in excess of 0.99. Another key characteristic of the concentric concept was the self-correction of instrument "smile", which was demonstrated to be negligible. The measurement of the atmospheric spectrum has also shown the potential of this spectrometer for DOAS applications when coupled with appropriate entrance optics.

Another significant output is the demonstration that the optical components for this type of spectrometer, principally the diffraction grating, can be manufactured to the necessary specification. The total integrated scatter from this critical part was found to be exceptionally good for such this component being the first of its kind, ranging from approximately 0.15% at 300 nm to 0.07% at 450 nm.

Acknowledgements. The authors would like to thank all the manufacturers of the components for their efforts on delivering the items to the specification and to the dedication of the university workshops in providing the substructure of the instrument. This work was funded by the NERC/TSB Centre for Earth Observation Instrumentation.

References

Aliwell, S. R., Van Roozendael, M., Johnston, P. V., Richter, A., Wagner, T., Arlander, D. W., Burrows, J. P., Fish, D. J., Jones, R. L., Tornkvist, K. K., Lambert, J. C., Pfeilsticker, K., and Pundt, I.: Analysis for BrO in zenith-sky spectra: An intercomparison exercise for analysis improvement, J. Geophys. Res.-Atmos., 107, 4199, doi:10.1029/2001JD000329, 2002.

Axelsson, H., Edner, H., Galle, B., Ragnarson, P., and Rudin, M.: Differential Optical-Absorption Spectroscopy (DOAS) Measurements of Ozone in the 280–290 nm Wavelength Region, Appl. Spectrosc., 44, 1654–1658, 1990.

Bobrowski, N., Honninger, G., Galle, B., and Platt, U.: Detection of bromine monoxide in a volcanic plume, Nature, 423, 273–276, doi:10.1038/nature01638, 2003.

Bobrowski, N. and Platt, U.: SO_2/BrO ratios studied in five volcanic plumes, J. Volcanol. Geoth. Res., 166, 147–160, doi:10.1016/j.jvolgeores.2007.07.003, 2007.

Bonay, M. and Aubier, M.: Air pollution and allergic airway diseases, MS-Medecine Sciences, 23, 187–192, 2007.

Bovensmann, H., Noël, S., Goede, A. P. H., and Burrows, J. P.: The Geostationary Scanning Imaging Absorption Spectrometer (GeoSCIA) mission: Requirements and Capabilities, Adv. Space Res., 29, 1849–1859, 2002.

Bovensmann, H., Eichmann, K. U., Noel, S., Flaud, J. M., Orphal, J., Monks, P. S., Corlett, G. K., Goede, A. P., von Clarmann, T., Steck, T., Rozanov, V., and Burrows, J. P.: The geostationary scanning imaging absorption spectrometer (GeoSCIA) as part of the geostationary tropospheric pollution explorer (GeoTROPE) mission: requirements, concepts and capabilities, in: Trace Constituents in the Troposphere and Lower Stratosphere, Adv. Space Res., 694–699, 2004.

Cai, X. M., Zheng, Y., and McGregor, G. R.: Modelling of meteorological conditions at an urban scale for the PUMA winter campaign, Phys. Chem. Earth, 27, 1479–1485, 2002.

Cardenas, L. M., Brassington, D. J., Allan, B. J., Coe, H., Alicke, B., Platt, U., Wilson, K. M., Plane, J. M. C., and Penkett, S. A.: Intercomparison of formaldehyde measurements in clean and polluted atmospheres, J. Atmos. Chem., 37, 53–80, 2000.

Edner, H., Ragnarson, P., Spannare, S., and Svanberg, S.: Differential Optical-Absorption Spectroscopy (DOAS) System for Urban Atmospheric-Pollution Monitoring, Appl. Optics, 32, 327–333, 1993.

Eskes, H., Tanskanen, A., Elbern, H., Buchwitz, M., Meirink, J. F., de Leeuw, G., Bovensmann, H., Valks, P., Meerkotter, R., Staiger, H., Fanton d'Andon, O., Kilbane Dawe, I., Holzer-Popp, T., Kyrola, E., Flaud, J.-M., Baier, F., Erbertseder, T., van Weele, M., and Flore, F.: S3 Service Prospectus, 2006.

Evangelisti, F., Baroncelli, A., Bonasoni, P., Giovanelli, G., and Ravegnani, F.: Differential Optical-Absorption Spectrometer for Measurement of Tropospheric Pollutants, Appl. Optics, 34, 2737–2744, 1995.

Friess, U., Wagner, T., Pundt, I., Pfeilsticker, K., and Platt, U.: Spectroscopic measurements of tropospheric iodine oxide at Neumayer Station, Antarctica, Geophys. Res. Lett., 28, 1941–1944, 2001.

Friess, U., Kreher, K., Johnston, P. V., and Platt, U.: Ground-based DOAS measurements of stratospheric trace gases at two Antarctic stations during the 2002 ozone hole period, J. Atmos. Sci., 62, 765–777, 2005.

Friess, U., Monks, P. S., Remedios, J. J., Rozanov, A., Sinreich, R., Wagner, T., and Platt, U.: MAX-DOAS O_4 measurements: A new technique to derive information on atmospheric aerosols: 2, Modeling studies, J. Geophys. Res.-Atmos., 111, D14203,

doi:10.1029/2005jd006618, 2006.
Harrison, R. M., Yin, J., Tilling, R. M., Cai, X., Seakins, P. W., Hopkins, J. R., Lansley, D. L., Lewis, A. C., Hunter, M. C., Heard, D. E., Carpenter, L. J., Creasy, D. J., Lee, J. D., Pilling, M. J., Carslaw, N., Emmerson, K. M., Redington, A., Derwent, R. G., Ryall, D., Mills, G., and Penkett, S. A.: Measurement and modelling of air pollution and atmospheric chemistry in the UK West Midlands conurbation: Overview of the PUMA Consortium project, Sci. Total Environ., 360, 5–25, 2006.
Hastings, W. P., Koehler, C. A., Bailey, E. L., and De Haan, D. O.: Secondary Organic Aerosol Formation by Glyoxal Hydration and Oligomer Formation: Humidity Effects and Equilibrium Shifts during Analysis, Environ. Sci. Technol., 39, 8728–8735, 2005.
Hönninger, G. and Platt, U.: Observations of BrO and its vertical distribution during surface ozone depletion at Alert, Atmos. Environ., 36, 2481–2489, 2002.
Hönninger, G., von Friedeburg, C., and Platt, U.: Multi axis differential optical absorption spectroscopy (MAX-DOAS), Atmos. Chem. Phys., 4, 231–254, 2004, http://www.atmos-chem-phys.net/4/231/2004/.
Kelder, H., van Weele, M., Goede, A., Kerridge, B., Reburn, J., Bovensmann, H., Monks, P., Remedios, J., Mager, R., Sassier, H., and Baillon, Y.: Operational Atmospheric Chemistry Monitoring Missions, European Space Agency, 2005.
Kim, S. W., Yoon, S. C., Won, J. G., and Choi, S. C.: Ground-based remote sensing measurements of aerosol and ozone in an urban area: A case study of mixing height evolution and its effect on ground-level ozone concentrations, Atmos. Environ., 41, 7069–7081, doi:10.1016/j.atmosenv.2007.04.063, 2007.
Kramer, L. J., Leigh, R. J., Remedios, J. J., and Monks, P. S.: Comparison of OMI and ground-based in situ and MAX-DOAS measurements of tropospheric nitrogen dioxide in an urban area, J. Geophys. Res.-Atmos., 113, doi:10.1029/2007jd009168, 2008.
Kuhl, S., Wilms-Grabe, W., Frankenberg, C., Grzegorski, M., Platt, U., and Wagner, T.: Comparison of OClO nadir measurements from SCIAMACHY and GOME, Atmospheric Remote Sensing: Earth's Surface, Troposphere, Stratosphere and Mesosphere – Ii, 37, 2247–2253, doi:10.1016/j.asr.2005.06.061, 2006.
Lee, J. S., Kim, Y. J., Kuk, B., Geyer, A., and Platt, U.: Simultaneous measurements of atmospheric pollutants and visibility with a long-path DOAS system in urban areas, Environ. Monit. Assess., 104, 281–293, doi:10.1007/s10661-005-1616-6, 2005.
Leigh, R. J., Corlett, G. K., Frie, U., and Monks, P. S.: Spatially resolved measurements

AMTD
2, 1901–1931, 2009

of nitrogen dioxide in an urban environment using concurrent multi-axis differential optical absorption spectroscopy, Atmos. Chem. Phys., 7, 4751–4762, 2007, http://www.atmos-chem-phys.net/7/4751/2007/.

Leser, H., Honninger, G., and Platt, U.: MAX-DOAS measurements of BrO and NO_2 in the marine boundary layer, Geophys. Res. Lett., 30, 1537, doi:10.1029/2002gl015811, 2003.

Lobb, D.: Theory of concentric designs for grating spectrometers, Appl. Optics, 33, 2648–2658, 1994.

Lobb, D.: Design of a spectrometer system for measurements on Earth atmosphere from geostationary orbit, in: Procedings of SPIE Optical Design and Engineering, edited by: Mazura, L., Rogers, P. J., and Wartmann, R., SPIE, 191–202, 2004.

Lohberger, F., Honninger, G., and Platt, U.: Ground-based imaging differential optical absorption spectroscopy of atmospheric gases, Appl. Optics, 43, 4711–4717, 2004.

Louban, I., Piriz, G., Platt, U., and Frins, E.: Differential Optical Absorption Spectroscopy (DOAS) using targets: SO_2 and NO_2 measurements in Montevideo city, Riao/Optilas 2007, 992, 21–26, 2008.

Mihailovic, D. T., Rao, S. T., Alapaty, K., Ku, J. Y., Arsenic, I., and Lalic, B.: A study on the effects of subgrid-scale representation of land use on the boundary layer evolution using a 1-D model, Environ. Modell. Softw., 20, 705–714, 2005.

Monks, P. S.: Tropospheric Photochemistry, in: Handbook of Atmospheric Science: Principles and Applications, edited by: Hewitt, C. N. and Jackson, A., Wiley-Blackwell, 2003.

Owen, B., Edmunds, H. A., Carruthers, D. J., and Raper, D. W.: Use of a new generation urban scale dispersion model to estimate the concentration of oxides of nitrogen and sulphur dioxide in a large urban area, Sci. Total Environ., 235, 277–291, 1999.

Palazzi, E., Petritoli, A., Ravegnani, F., Kostadinov, I., Bortoli, D., Masieri, S., Premuda, M., and Giovanelli, G.: Multiple axis DOAS measurements for the retrieval of nitrogen dioxide and ozone vertical profiles in the Presidential Estate of Castel Porziano (Rome) – Conference on Remote Sensing of Clouds and the Atmosphere XII, Florence, ITALY, art. no. 67451Y ISI:000253868600053, Y7451, 2007.

Platt, U.: Differential optical absorption spectroscopy, (DOAS), in air monitoring by spectroscopic techniques, in: Chemical Analysis, edited by: Sigrist, M. W., Wiley, New York, 1994.

Prieto-Blanco, X., Montero-Orille, C., Couce, B., and de la Fuente, R.: Analytical design of an Offner imaging spectrometer, Opt. Express, 14, 9156–9168, 2006.

Pundt, I., Mettendorf, K. U., Laepple, T., Knab, V., Xie, P., Losch, J., Friedeburg, C. V.,

Platt, U., and Wagner, T.: Measurements of trace gas distributions using Long-path DOAS-Tomography during the motorway campaign BAB II: experimental setup and results for NO_2, Atmos. Environ., 39, 967–975, doi:10.1016/j.atmosenv.2004.07.035, 2005.

Richter, A., Eisinger, M., Ladstatter-Weissenmayer, A., and Burrows, J. P.: DOAS Zenith sky observations: 2. Seasonal variation of BrO over Bremen (53 degrees N) 1994–1995, J. Atmos. Chem., 32, 83–99, 1999.

Sinreich, R., Friess, U., Wagner, T., and Platt, U.: Multi axis differential optical absorption spectroscopy (MAX-DOAS) of gas and aerosol distributions, Faraday Discuss., 130, 153–164, doi:10.1039/b419274p, 2005.

Tornkvist, K. K., Arlander, D. W., and Sinnhuber, B.-M.: Ground-based UV measurements of BrO and OClO over Ny-Alesund during winter 1996 and 1997 and Andoya during winter 1998/99, J. Atmos. Chem., 43, 75–106, 2002.

Van Roozendael, M., Hermans, C., Demaziere, M., and Simon, P. C.: Stratospheric NO_2 observations at the Jungfraujoch Station between June 1990 and May 1992, Geophys. Res. Lett., 21, 1383–1386, 1994.

Veitel, H., Kromer, B., Mossner, M., and Platt, U.: New techniques for measurements of atmospheric vertical trace gas profiles using DOAS, Environ. Sci. Pollut. R., 4, 17–26, 2002.

Virkkula, A.: Performance of a differential optical absorption spectrometer for surface O–3 measurements in the Finnish Arctic, Atmos. Environ., 31, 545–555, 1997.

Wagner, T., Dix, B., von Friedeburg, C., Friess, U., Sanghavi, S., Sinreich, R., and Platt, U.: MAX-DOAS O_4 measurements: A new technique to derive information on atmospheric aerosols – Principles and information content, J. Geophys. Res.-Atmos., 109, D22205, doi:10.1029/2004jd004904, 2004.

Wang, S., Ackermann, R., and Stutz, J.: Vertical profiles of O_3 and NO_x chemistry in the polluted nocturnal boundary layer in Phoenix, AZ: I. Field observations by long-path DOAS, Atmos. Chem. Phys., 6, 2671–2693, 2006, http://www.atmos-chem-phys.net/6/2671/2006/.

Wittrock, F., Muller, R., Richter, A., Bovensmann, H., and Burrows, J. P.: Measurements of iodine monoxide (IO) above Spitsbergen, Geophys. Res. Lett., 27, 1471–1474, 2000.

Table 1. Estimated total integrated scatter for CompAQS instrument evaluated from the total contribution from each component, assuming a worst case scenario of 0.1% from the lens in the absence of subsurface quality information.

Component TIS Contribution / %	Wavelength / nm 300	320	350	370	400	425	450
Grating	0.1518	0.1293	0.1115	0.0971	0.0854	0.0756	0.0674
Lens	0.1	0.1	0.1	0.1	0.1	0.1	0.1
Spherical Mirror	0.0846	0.0721	0.0622	0.0541	0.0476	0.0422	0.0376
Fold MIrror	0.1755	0.1542	0.1289	0.1153	0.0987	0.0874	0.0780
Instrument Total Integrated Scatter / %	0.5118	0.4556	0.4026	0.3666	0.3316	0.3052	0.2830

AMTD
2, 1901–1931, 2009

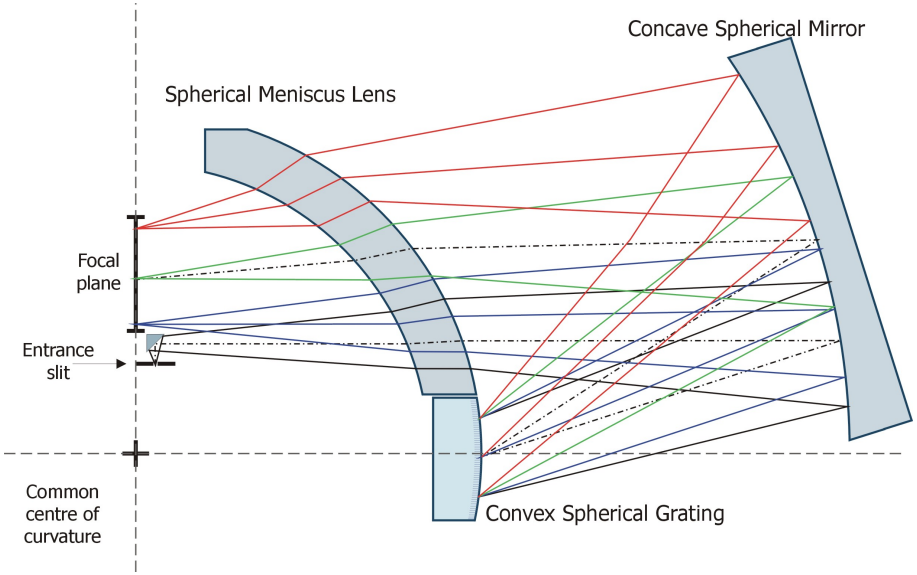

Fig. 1. The Lobb design for a novel reduced size concentric spectrometer. This diagram is adapted from Lobb (2004).

AMTD
2, 1901–1931, 2009

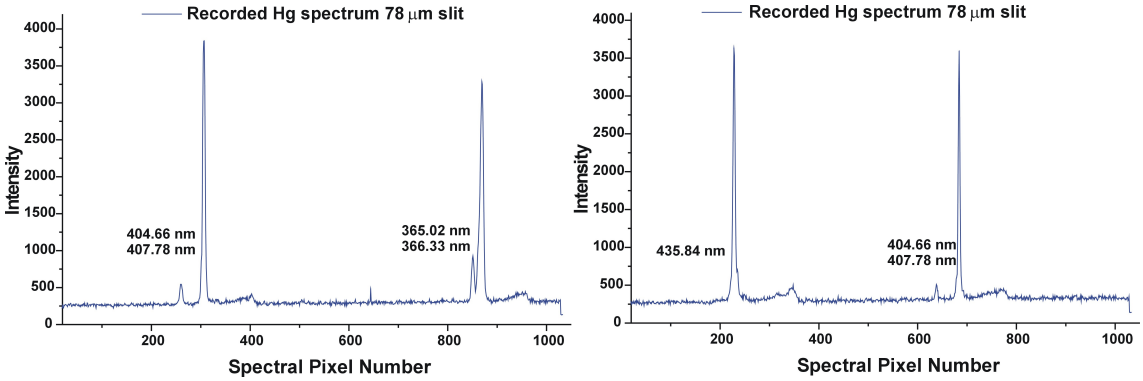

Fig. 2. The mercury line spectra recorded in the first light optimisation experiments for the 78 μm slits.

AMTD
2, 1901–1931, 2009

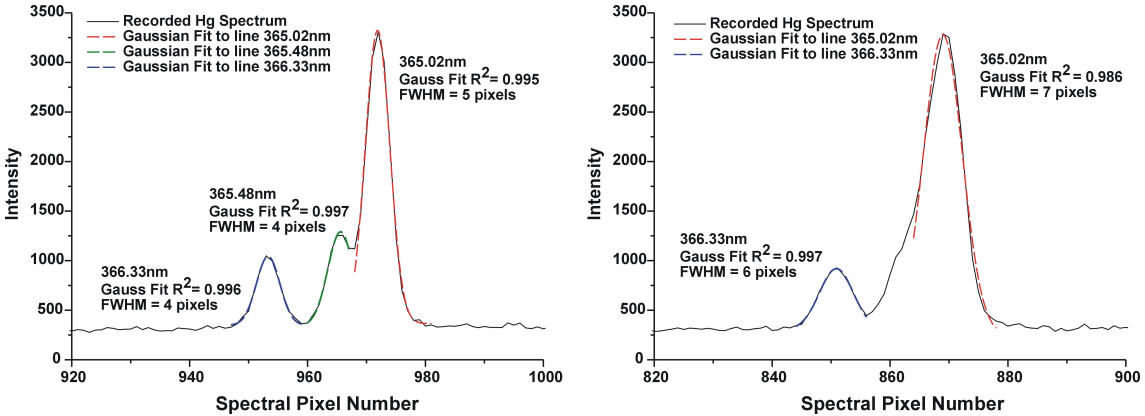

Fig. 3. A closer examination of the 365 nm lines recorded for slit widths of 65 μm (left) and 78 μm (right).

AMTD
2, 1901–1931, 2009

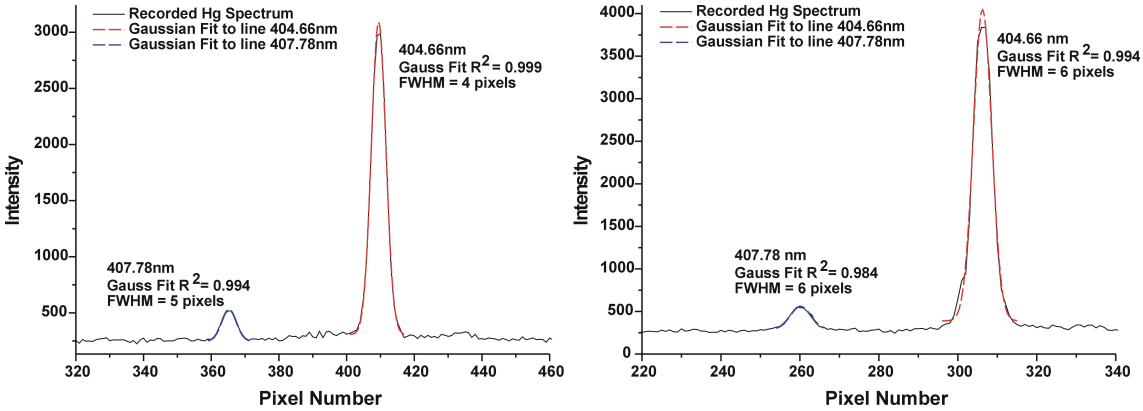

Fig. 4. A closer examination of the 404 and 407 nm line recorded for slit widths of 65 μm (left) and 78 μm (right).

AMTD
2, 1901–1931, 2009

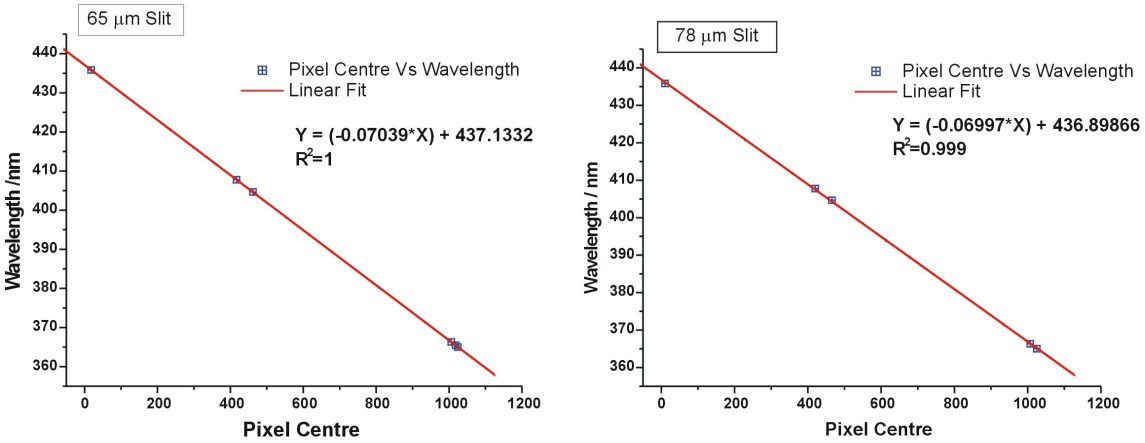

Fig. 5. Wavelength calibration plots for the 65 μm slit (top) and the 78 μm slit (bottom) showing the linear fit applied to each data set.

AMTD
2, 1901–1931, 2009

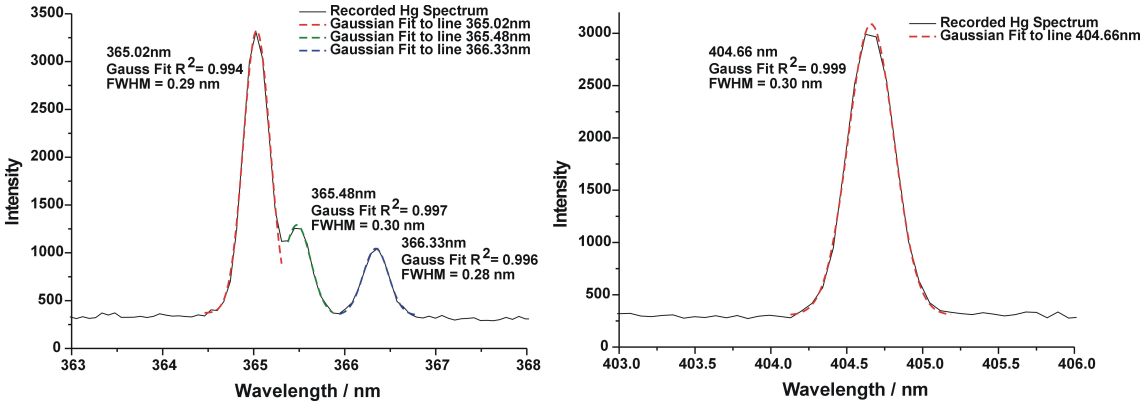

Fig. 6. Wavelength calibrated mercury emission lines with Gaussian fits applied to each emission line for data recorded with the 65 μm slit.

AMTD
2, 1901–1931, 2009

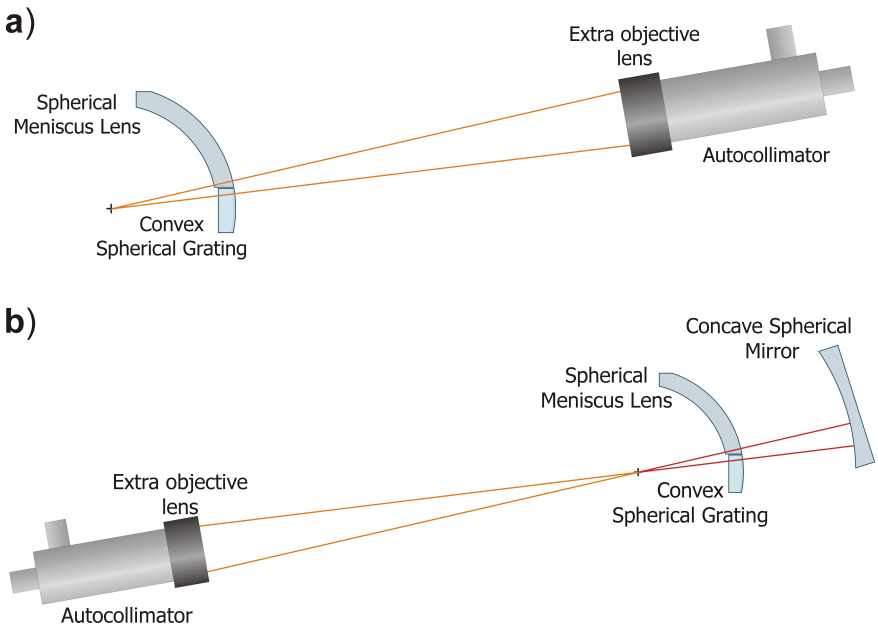

Fig. 7. The alignment of the concentric optical components using an adapted autocollimator fitted with an additional objective lens: **(a)** aligning the meniscus lens with the grating and the centre of curvature; **(b)** aligning the concave mirror with the grating and meniscus lens.

AMTD
2, 1901–1931, 2009

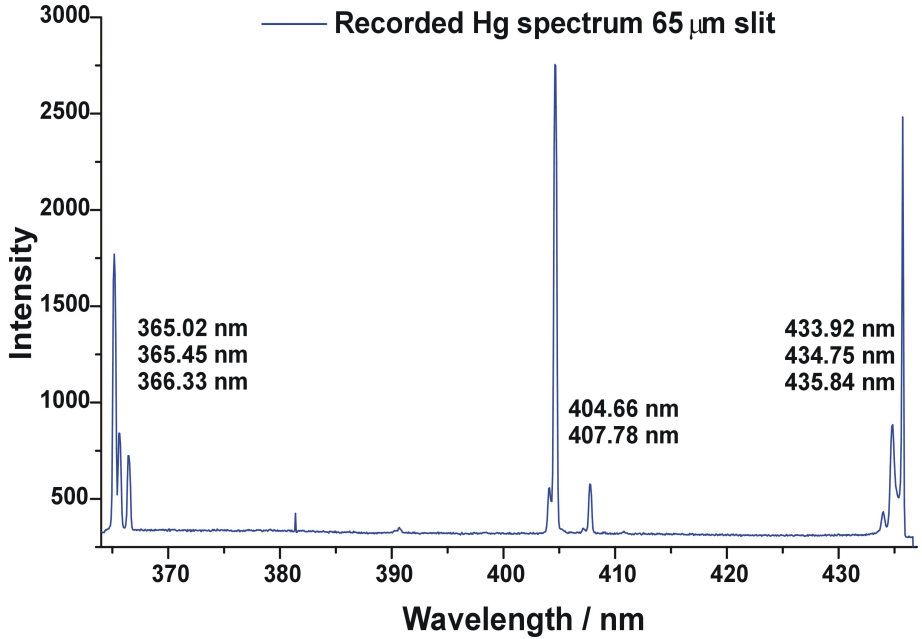

Fig. 8. An example of a mercury emission spectrum recorded from the CompAQS instrument with the concentric optical components fully aligned and confirmed.

AMTD
2, 1901–1931, 2009

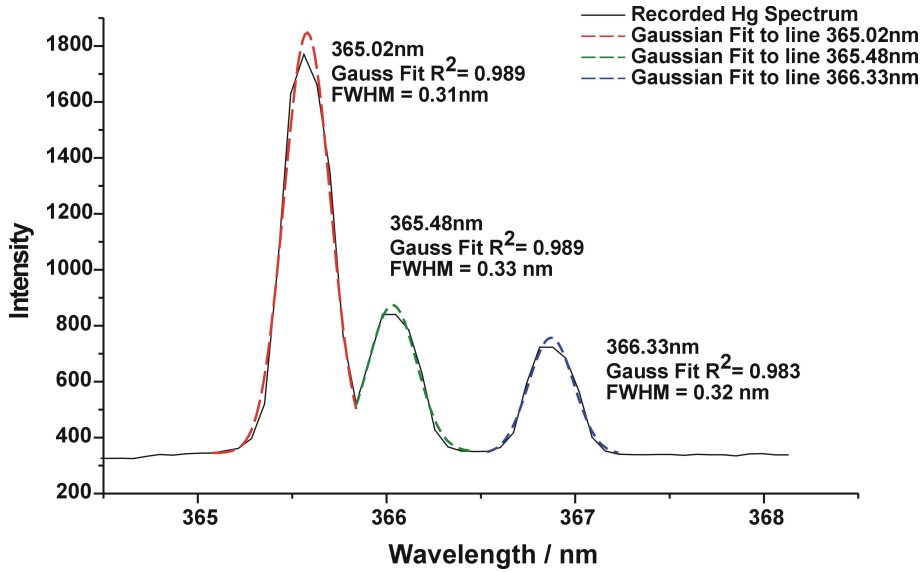

Fig. 9. A closer view of the 365 mercury emission lines recorded with the 65 μm slit, showing Gaussian fits to the peak shapes and a resolution of ~0.3 nm.

AMTD
2, 1901–1931, 2009

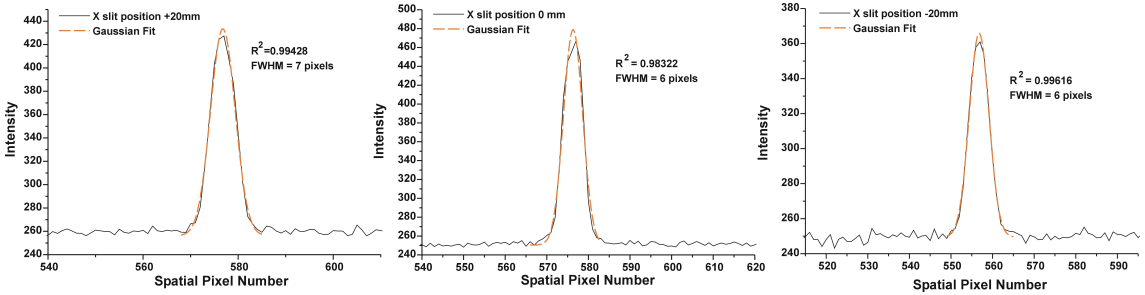

Fig. 10. A collection of the spatially resolved elements from the 404.66 nm mercury emission line for different locations of the entrance slit.

AMTD
2, 1901–1931, 2009

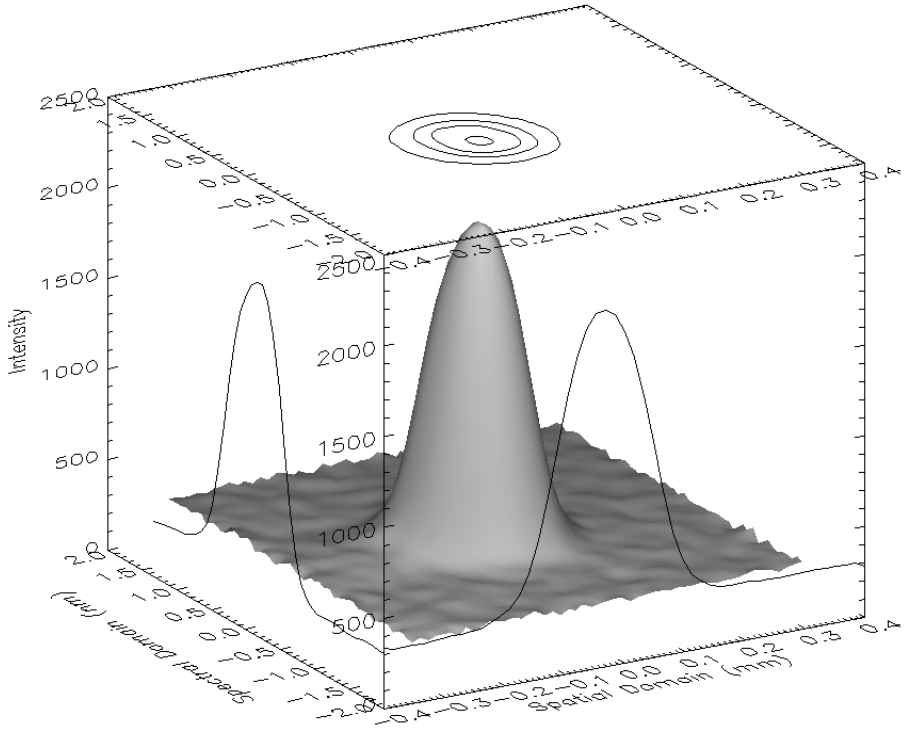

Fig. 11. A 3-D representation of the spatially resolved 404.66 nm mercury emission.

AMTD
2, 1901–1931, 2009

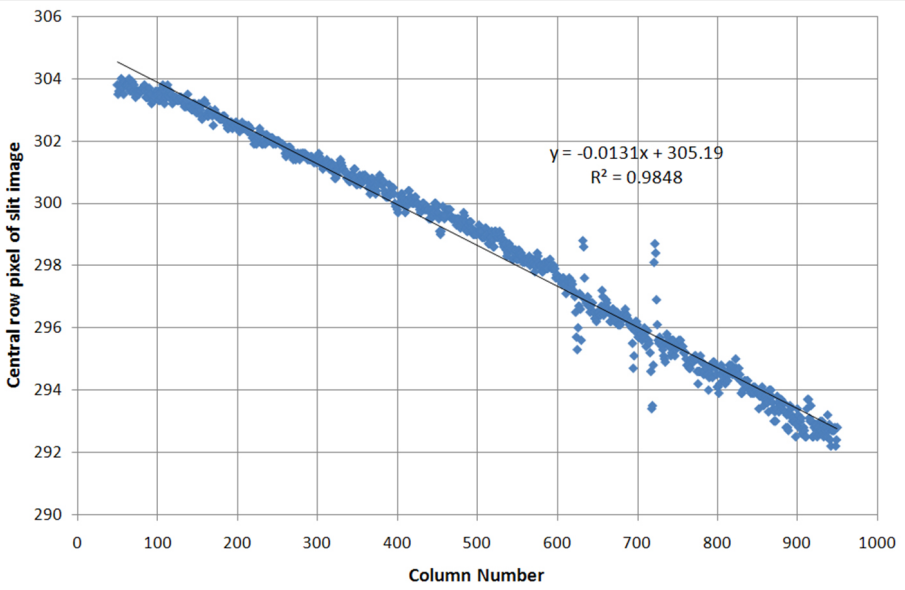

Fig. 12. A measurement of the "smile" in the CompAQS spectrometer system. The overall slope of the plot is due to a minor rotation of the CCD detector with respect to the focal plane. Sub-pixel values were obtained using a combined smoothing/spline interpolation routine. Features around column 620 and 710 result from artefacts on the CCD surface, and not deviation of the image.

AMTD
2, 1901–1931, 2009

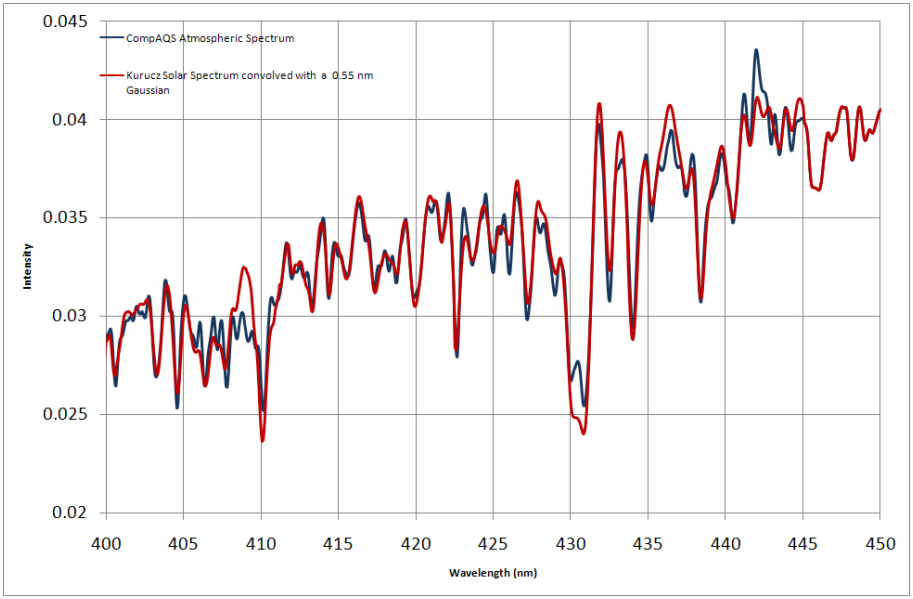

Fig. 13. Example atmospheric spectrum from the CompAQS instrument, plotted with a convolved Kurucz solar spectrum at 0.55 nm.

AMTD
2, 1901–1931, 2009